Journal of the Faculty of Environmental Science and Technology, Okayama University
Vol 5, No.1, pp. 81-98, February 2000

Floatation of Buried Submarine Pipeline under Cyclic Loading of Water Pressure —Numerical and Experimental Studies—

Waldemar MAGDA*, Shiro MAENO** and Hiroshi NAGO**

(Received January 18 , 2000)

A dynamic response of a submarine pipeline buried in sandy seabed sediments to water loading generated by harmonically oscillating water-table vertical movements is examined in the present report experimentally and numerically. The aim of small-scale laboratory experiments was: (1) to record time-histories of pipeline vertical displacements, and (2) to observe a shape of slip surface of an overburden sand body involved in breakout together with the pipeline. A parametric study was carried out in order to investigate the influence of two meaningful factors, that is the depth of burial and the specific gravity of pipeline, on a gradual upward displacement of the pipeline. Based on a numerical finite-element 2D-analysis of the hydrodynamic pore pressure and effective stresses oscillations in the pipeline vicinity, an analysis of the pipeline stability potential is presented, in which all the experimental cases tested are verified. All important component forces (*e.g.*, hydrodynamic uplift force) associated with floatation phenomenon of the buried submarine pipeline are considered and quantified.

Key words: *submarine pipeline, surface waves, pore pressure, floatation, stability.*

1 INTRODUCTION

Submarine pipelines have been continuously considered as the most efficient and economic means of transport of crude oil and natural gas from offshore fields to land basis. An increasing need for exploration and exploitation of hydrocarbon reserves under the continental shelf is responsible for the fact that many new submarine pipelines are just under construction, and many others undergo design procedures. As far as shallow-water regions are concerned, it is normal for the engineering practice that submarine pipelines located in a coastal zone (*i.e.*, in water depth up to approx 60 m) are buried (trenched), whereas the cover soil layer resting above the pipeline must have a thickness ranging from 0.5 to 1.0 m (Dursthoff and Mazurkiewicz, 1985). The main reason to bury pipelines is to protect them from any hydrodynamic (*e.g.*, wave-induced uplift and drag forces, wave-induced submarine slope instability) or/and mechanical (*e.g.*, fishing gear, ship's anchor) damage. Burial of the pipeline in seabed sediments helps to counteract the pipeline instability. However, due to the effect of dynamic pressure waves on the ocean floor, caused by surface water waves, dynamic loads are exerted on the buried pipeline. Surface water waves, generated especially during a storm appearance, can create high-amplitude oscillations of the wave-induced pore pressure in sandy seabed sediments, which, in turn, can increase a hydrodynamic uplift force acting to a submarine buried pipeline (Fig. 1), decreasing simultaneously resistant forces, influencing thereby the potential of pipeline floatation. Therefore, one of the main design requirements to be fulfilled is that the submarine buried pipeline should not float upward during its installation and operational phases.

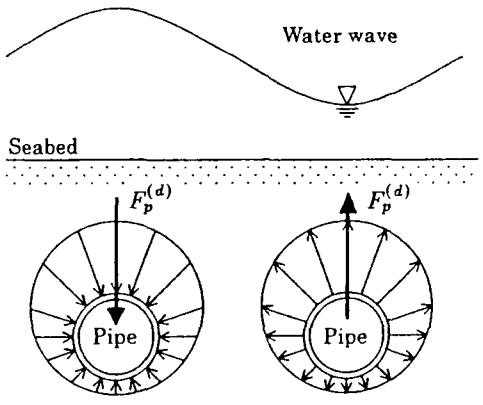

(a) Wave crest (b) Wave trough

Fig. 1 Wave-induced pore pressure distributions around pipeline circumferential for crest- and trough-phase of surface water wave loading

* Marine Civil Engineering Department, Faculty of Environmental Engineering, Technical University of Gdansk, Gdansk, Poland
** Department of Environmental and Civil Engineering, Faculty of Environmental Science and Technology, Okayama University, Okayama, Japan.

An inadequate design may cause floatation of the pipeline, very often leading to subsequentially to costly pipeline failures and environmental catastrophies. Therefore, it is essential to improve continuously our engineering knowledge and experience on interactions between water waves, seabed, and submarine buried pipeline.

2 A BRIEF LITERATURE REVIEW

A wave-induced oscillating pore pressure, generated in the vicinity of a submarine buried pipeline, constitutes one of the main factors that has to be considered in the pipeline stability analysis. The maximum hydrodynamic uplift force acting on the pipeline is comparable to the displaced water weight (Monkmeyer *et al.*, 1983; Cheng & Liu, 1986; Magda, 1992, 1998) if the pipeline is located relatively close to the seabed floor. Therefore, many publications have already been devoted to the wave-induced uplift force solutions. However, only a few of them (*e.g.*: Bobby *et al.*, 1979; Cheng & Liu, 1986; Magda, 1997) pertained to the most relevant case for engineering practice, where seabed sediments can be treated as a compressible two-phase (pore-fluid/soil-skeleton) medium. Magda (1997) presented a thorough analysis of numerical (FEM) results, putting a special attention to the influence of pore fluid compressibility (soil saturation conditions, indirectly); this treatment allowed for a definition of the maximum wave-induced uplift force with respect to compressibility properties of the seabed.

Besides the wave-induced uplift force, another factor that one has to consider in the pipeline floatation analysis is the resistance (restraint) created by the pipeline covering soil layer against the upward movement of the pipeline. A review of vertical and horizontal soil restraints of buried pipelines was given by Audibert *et al.* (1978). Nyman (1982) extended Meyerhof's model for the behaviour of soil restraint for inclined strip anchors to buried circular pipelines. However, considering a very special case thereof, *i.e.* the vertical uplift pipeline restraint problem, which is typical for the stability analysis of submarine buried pipelines, a solution by Vesic (1971) developed for the expansion of cylindrical cavities close to the surface of a semi-infinite plastic soil can be used. It has to be emphasized that the above citied studies were related to the case where the soil was not saturated. In saturated soils (*e.g.*, sandy seabed sediments) not only the pull-out force (animated by the wave-induced uplift force acting on the pipeline) is present, but also additional wave-induced dynamic forces act to the covering soil layer due to certain wave-induced pore pressure and effective stresses distributions in the pipeline/seabed vicinity.

Siddharthan & Norris (1993) identified all the important factors associated with pipeline floatation mechanisms and provided methods and guidelines to quantify these factors with the main consideration given to the wave-induced residual pore pressure (*i.e.*, pore pressure buildup due to some plastic deformations of the seabed skeleton induced by storm water waves). They also demonstrated their approach, including a numerical example computed for the North Sea wave and soil conditions.

Large-scale experiments with buried pipelines are estimated to be rather ineffective (difficult to be carried out and very expensive) as far as parameter studies are concerned. Therefore, only small-scale laboratory modelling has been reported in the literature. One of the latest is given by Pranesh & Raghava Rao (1997), who investigated the hydrodynamic pore pressure on a pipeline buried in sand bed due to the action of progressive surface water waves, modelling different geometry of the system by changing: wave period, wave height, water depth, and the depth of burial. The pipeline model was clamped at the both ends of the test section to prevent any movements (a "fixed-pipeline" case). Magda *et al.* (1996) and Maeno *et al.* (1997) studied the dynamic pore pressure around a buried pipeline loaded by a vertically oscillating water-table movement, varying the period of water loading oscillations and introducing different soil permeabilities. In the above mentioned experimental studies, seepage forces acting on the pipeline were calculated by integrating the dynamic pore pressure distributions measured along the pipeline circumferential. Additionally, Pranesh & Raghava Rao (1997) concluded that the relative seabed thickness factor (RST), which is the ratio of total seabed thickness to wavelength, has a predominant influence on the wave-induced pore pressure arond the buried pipeline. Magda *et al.* (1998) verified the experimental results using the finite-element 2D-modelling and indicated near-fully saturation conditions ($S = 0.992 - 0.998$, where S is the degree of saturation) in the seabed model.

3 EXPERIMENTAL INVESTIGATION

Two different types of small-scale experimental investigations have been performed in order to study the floatation phenomenon of a submarine pipeline buried in sandy seabed sediments and loaded by surface water waves. The two types of experiments can be distinguished as:

- pipeline floatation tests (dynamic tests),
- pull-out tests (static tests).

The pipeline floatation dynamic tests were established to record a time-history of the pipeline vertical displacement due to cyclically oscillating water loading. The aim of the static pull-out tests, performed under a static water level, was to measure a minimum value of the pull-out force required to initiate an upward movement of the pipeline. A second reason to carry out the static tests was to observe a shape of

slip surfaces (*i.e.*, shear failure lines) within the covering soil layer involved in breakout together with the pipeline during its initial movement upwards.

3.1 Test facilities and layout

The experimental facilities designed for the pipeline floatation dynamic tests are shown in Fig. 2. A rectangular sand container has the following dimensions: $L_c = 1.0\,\mathrm{m}$ (length), $H_c = 0.7\,\mathrm{m}$ (height), and $B_c = 0.4\,\mathrm{m}$ (width). The container was filled with highly saturated sand. The thickness of the sand layer is $H_s = 0.6\,\mathrm{m}$. The small-scale test facilities did not allow to load the model by progressive surface water waves. Therefore, on the top of the sand container, an oscillating water column was installed, in which a still water level (measured from the sand surface) was equal to $d = 1.2\,\mathrm{m}$. The water-table vertical oscillations in the column were generated by an oscillating air pressure acting on the water surface. The air pressure oscillations, in turn, were produced by a mechanical/hydraulic generator. The amplitude of cyclic water pressure oscillations was equal $A = 0.4\,\mathrm{m}$, whereas the period of oscillations was equal $T = 1.0\,\mathrm{s}$.

A cylindrical and hardly deformable element of the pipeline, made of perspex, was buried in the sand box parallel to the longer side of the box (see Fig. 2). The outside diameter of the pipeline testing section equals $D_o = 0.1\,\mathrm{m}$ (the outer radius of the pipeline $r_p = D_o/2 = 0.05\,\mathrm{m}$), and the length was $L_p = 0.38\,\mathrm{m}$. Two measuring rods were mounteded vertically on the both ends of the pipeline in order to enable continuous monitoring of the pipeline vertical displacements, which were read out using a precise geodesic levelling instrument.

Three different depths of burial of the pipeline (measured from the seabed level to the top of the pipeline) were tested, namely: $b = 0.025$, 0.050, and $0.075\,\mathrm{m}$. For the case of a possibly wide parameter study of the pipeline floatation behaviour, five different specific gravities of the pipeline were modelled, that is: $G_p = 0.5$, 0.7, 0.9, 1.0, and 1.5. It has to be noted that the specific gravity $G_p < 1$ can be easily found in cases of submarine pipelines designed for a natural gas transport (*i.e.*, gas pipelines).

The experimental setup designed for the pull-out static tests is presented in Fig. 3. Basically, the same facilities, as in the pipeline floatation dynamic tests, were used. The static water conditions (a still water level was kept constant few centimetres above the sand surface) did not require the whole water-table oscillating system. However, an additional lifting device had to be installed, consisting of a wire going through a 2-roller-frame, and connecting the pipeline with the static weight container. The lifting system allowed the pipeline for a $0.02\,\mathrm{m}$ vertical displacement due to a stepwise application of a gravitational force into the static weigth container. In all the static pull-out experiments, the specific gravity of the pipeline was constant and equal $G_p = 1.0$.

3.2 Sand properties

The sand container was filled with a fine-grained type of sand ("Toyoura" standard sand; $d_{50} = 0.25$ mm). The specific gravity of the sand particles was equal $G_s = 2.649$, the coefficient of permeability $k = 1.5 \times 10^{-4}\,\mathrm{m/s}$, the porosity $n = 0.4$, Poisson's ratio $\nu = 0.4$, and the shear modulus $G = 3.5 \times 10^4\,\mathrm{kPa}$ [Young's modulus $E = 2(1+\nu)G = 1.015 \times 10^5\,\mathrm{kPa}$]. Additionally: the void ratio $e = n/(1-n) = 0.67$, and the buoyant unit weight $\gamma' = \gamma_w\,(G_s - 1)/(1+e) = 9.69\,\mathrm{kN/m^3}$, assuming the unit weight of water to be $\gamma_w = 9.81\,\mathrm{kN/m^3}$. For the purpose of the static pull-out tests, a coloured sand of the same type was used.

3.3 Test preparation procedure

The sand container was filled with water gradually. Between the two following water fillings, a certain volume of the dried sand was dropped freely into the water to assure repeatedly uniform soil conditions for each new-established test. A very careful preparation of the sand model required that the sand surface was always kept below the water surface. Using this procedure it was possible to achieve a high degree and uniformity of soil saturation, which was very meaningful for the pipeline floatation dynamic tests. It is very difficult to measure soil saturation conditions very precisely. It was clear that the sand model was highly but partly saturated. On the other hand it is well-known (Magda, 1997) that the seabed saturation conditions have a decisive influence on the hydrodynamic uplift force acting on the buried pipeline. Therefore, one of the most important goals in the test preparation procedure was to create sand saturation as high as possible (*i.e.*, near-fully saturated soil conditions) because, under these conditions, the saturation uniformity can be relatively easily obtained. An additional unit with a vibrating needle was used in order to release air-bubbles entrapped in the seabed model.

For the purpose of the static pull-out tests, a carefull preparation of the seabed model was essential starting from the pipeline bottom level upwards. The soil saturation conditions were believed not to be meaningful for the experimental results. The coloured sand was placed in a layered manner; counting from the depth of the pipeline centre, $0.01\,\mathrm{m}$ coloured sand layer, $0.02\,\mathrm{m}$ normal sand layer, *etc.*, up to the sand surface.

3.4 Results of pipeline floatation dynamic tests

All together 8 small-scale experiments with the free-movable pipeline were performed. During all the tests, two parameters were varied, *i.e.*: depth of burial, b, and specific gravity, G_p, of the pipeline. The values of these parameters tested are given in Tab. 1, respectively to the following experiments. In Case 2, a high permeable soil (fine gravel: $k = 2.045 \times 10^{-2}\,\mathrm{m/s}$, $d_{\%} = 2.83 - 3.36\,\mathrm{mm}$) was used in the model pipeline vicinity.

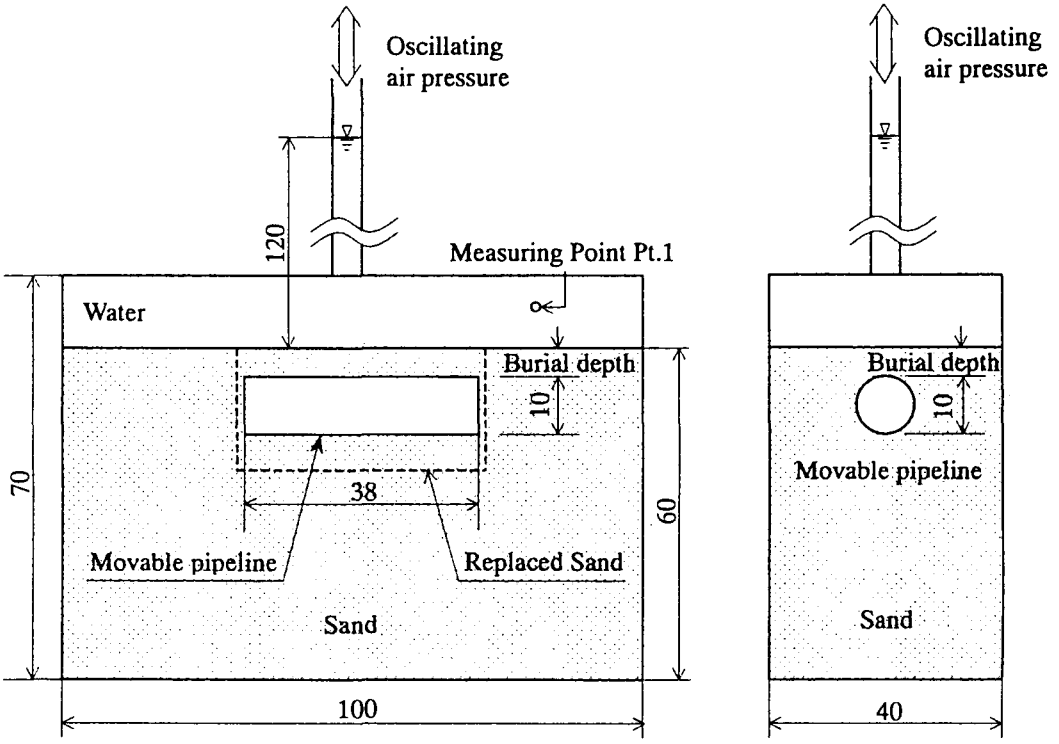

Fig. 2 Test facilities used in pipeline floatation dynamic tests (unit : cm)

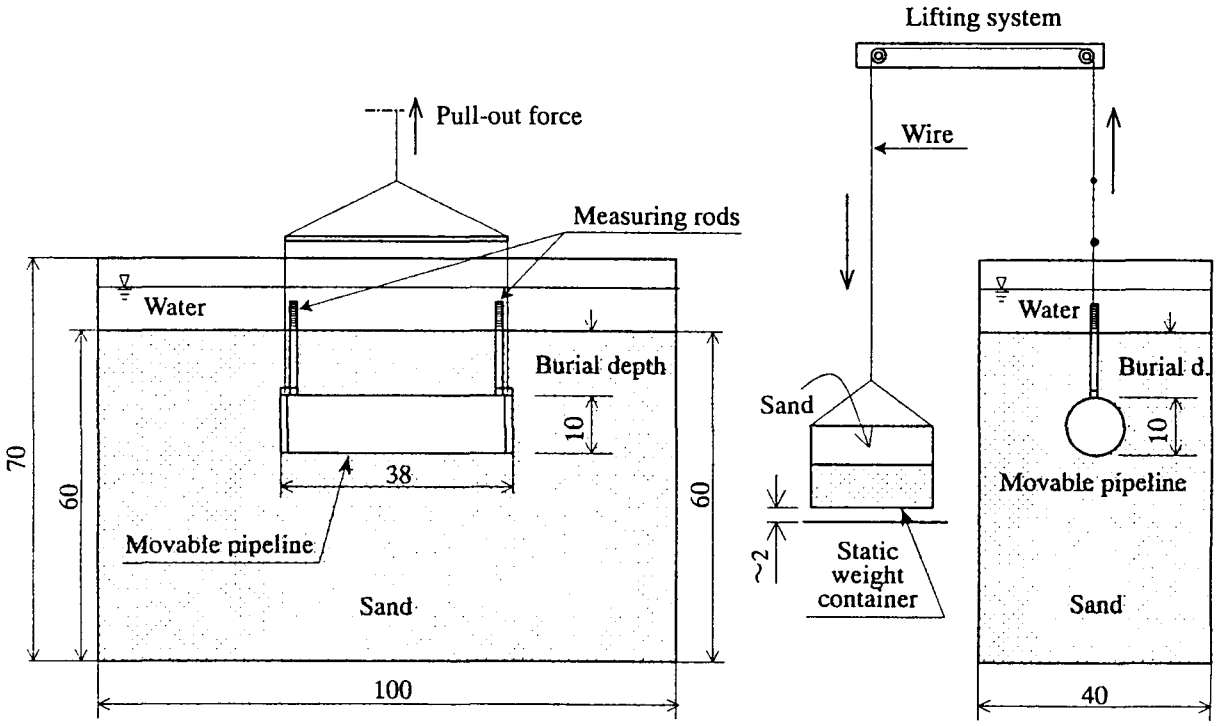

Fig. 3 Test facilities used in pull-out static tests (unit : cm)

Table 1 Set of parameters tested in the pipeline floatation dynamic tests.

Case	Depth of burial b [m]	Specific gravity G_p [-]
1	0.05	0.5
2	0.05	$0.5^{(*)}$
3	0.025	0.5
4	0.075	0.5
5	0.05	0.7
6	0.05	0.9
7	0.05	1.0
8	0.05	1.5

$(*)$ high permeable soil

Figure 4 shows the pore pressure (h in cm of water column) around the pipeline measured within one period of water-table oscillations. Although these measurements were performed in the fixed pipeline tests (Maeno *et al.*, 1997; Magda *et al.*, 1998), the illustrated case is representative to Case 1 (see Tab. 1) in the free-movable pipeline tests. Using simple integration of the hydrodynamic pore pressure around the pipeline circumference, the hydrodynamic uplift force, $F_p^{(d)}$ was computed. The order of the maximum hydrodynamic uplift force is about $F_p^{(d)} = 0.1\,\mathrm{kN/m}$, which appears during the apogee of the falling state of water pressure loading on the sand surface.

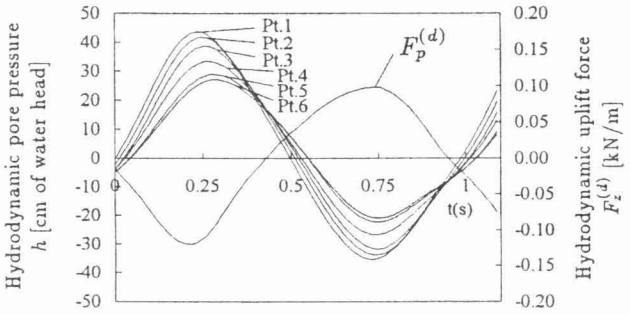

Fig. 4 Time-history of the wave-induced pore pressure, h, measured on the pipeline circumference (Pt.1 – bottom pressure, Pt.2 – pipe top, Pt.4 – pipe centre, Pt.6 – pipe bottom), and the hydrodynamic uplift force, $F_p^{(d)}$, computed numerically ('fixed-pipeline' test)

Figure 5 illustrates the time-history of the pipeline floatation dynamic test Case 1. As it can be seen, the pipeline gradually lifted up in the first stage of the experiment ($t = 0 - 25$ min). After that, the pipeline upward displacement seems to be accelerated and ended up with a sudden floatation of the pipeline onto the sand surface at $t = 53$ min of the test run.

Photo 1 shows the result of an extra movable-pipeline test carried out under the same experimental conditions as in Case 1. In this experiment, the coloured sand was arranged around the pipeline to visualize the movement of the pipeline and the sand

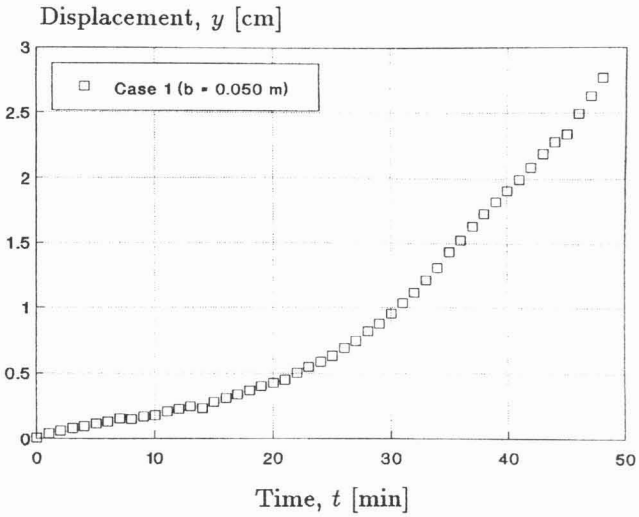

Fig. 5 Time-history of pipeline upward displacement in the pipeline floatation dynamic test (Case 1)

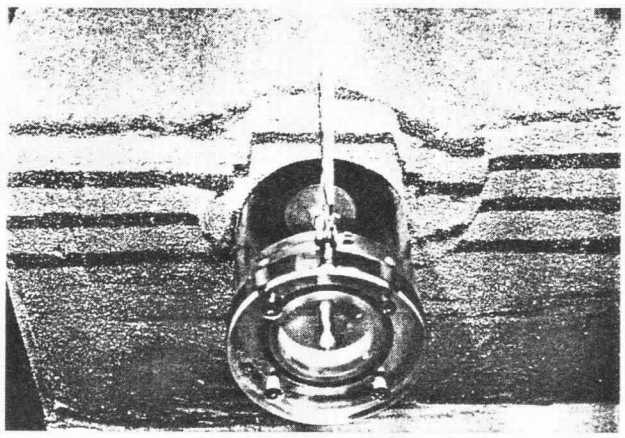

Photo 1 Cross-section of sand from the pipeline vicinity (coloured and layered sand)

involved in breakout. The sand movement is limited within the closest vicinity of the pipeline.

Figure 6 demonstrates the influence of introduction of the high permeable soil into the pipeline vicinity (Case 2) in comparison to Case 1. A soil of a relatively higher permeability does not contribute to magnification of pore pressure damping effects. Therefore, the hydrodynamic pore pressure gradient, and consequently the hydrodynamic uplift force, are smaller than in less permeable soils. In Case 2, the hydrodynamic uplift force, and also other forces, were not in a position to overcome the global resistance force even after a long time of the test run. The pipeline was continuously stable, whereas only small vertical downward movements of the pipeline were observed, thereby increasing slightly and additionally the pipeline stability.

Figure 7 presents the results of the three tests (Cases 3, 1, and 4) performed to study the influence of the depth of burial $b = 0.025$, 0.05, and 0.075 m,

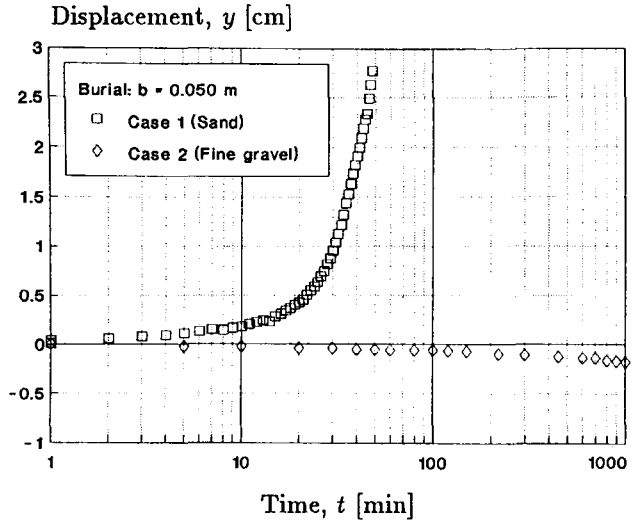

Fig. 6 Time-history of pipeline upward displacement in the pipeline floatation dynamic test (Case 2: high permeable soil in pipeline vicinity)

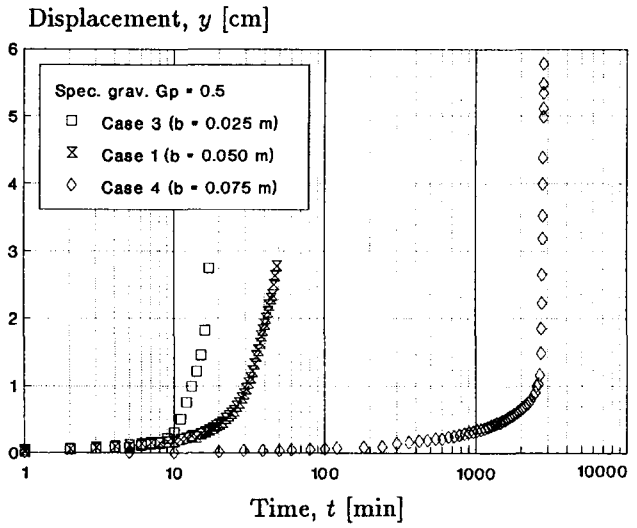

Fig. 7 Influence of the depth of burial on pipeline stability

respectively. All the 3 test results inform about the pipeline instability, indicating simultaneously the following expected trend: the deeper depth of burial the longer time is needed to obtain significant upward displacements. In Case 3 and Case 1, a relatively short time was necessary to lift up the pipeline leading to its floatation. In Case 4, a very small and slow gradual increase in the pipeline upward displacement was observed up to approximatelly $t = 2,700$ min when a crucial point was reached and the pipeline upward movement was accelerated from that time on, leading very soon to significant displacemens causing floatation of the pipeline.

Another comparison analysis is shown in Fig. 8 where the meaning of the pipeline specific gravity was investigated in 5 tests (Cases: 1, 5, 6, 7, and 8). The

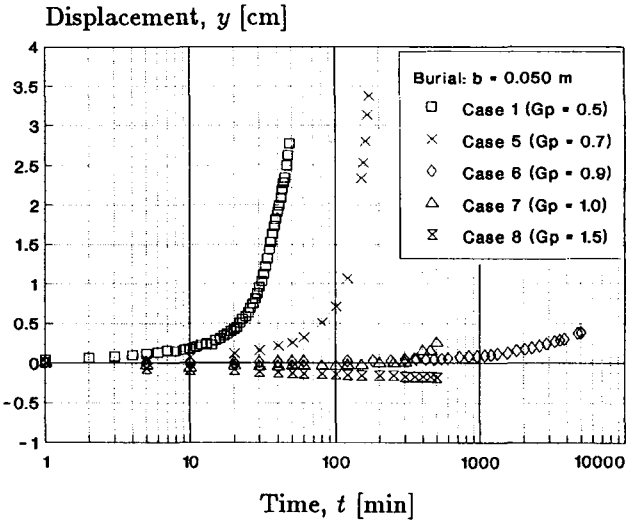

Fig. 8 Influence of the pipeline specific gravity on pipeline stability

specific gravity was stepwise increase starting from $G_p = 0.5$ (Case 1) to $G_p = 1.5$ (Case 8). As expected, the smaller effective weight of the pipeline, modelled by smaller values of the pipeline specific gravity, G_p, contributes to smaller resistance forces in the pipeline stability system, leading thereby to a faster rate of the upward displacement of the pipeline. For certain geometry and water loading conditions, there is somewhere a limit value for the specific gravity enabling to distinguish between stability and instability of the pipeline. From all the cases tested one can recognize that the specific gravity $G_p = 0.9$ (Case 6) and $G_p = 1.0$ (Case 7) can be considered as the limiting values. Application of the relatively larger effective weight of the pipeline (Case 8: $G_p = 1.5$) does not induce any pipeline instability, and even very small downward displacements were observed.

In the following, a computational analysis of the pipeline stability with respect to the above mentioned 8 cases of the free-movable pipeline tests will be given.

4 ANALYSIS OF PIPELINE VERTICAL STABILITY (FLOATATION)

Siddharthan & Norris (1993) discussed forces that have to be taken into account when assessing a stability criterion against floatation of pipelines buried in sandy soils. Introducing some necessary modifications, mainly due to the presence of pore pressure oscillations instead of pore pressure buildup, the component forces in the governing system can be depicted as follows (Fig. 9):

- the effective weight of the pipeline:
  - weight of the pipeline together with a medium transported, $W_p^{(g)}$,
  - hydrostatic component of the uplift force, $F_p^{(s)}$, acting on the pipeline,

  - hydrodynamic component of the uplift force, $F_p^{(d)}$, acting on the pipeline,
- the effective weight of the mass of soil involved in breakout together with the pipeline:
  - weight of the soil body involved in breakout, $W_s^{(g)}$,
  - hydrostatic component of the uplift force, $F_s^{(s)}$, acting on the soil skeleton,
  - hydrodynamic component of the uplift force, $F_s^{(d)}$, acting on the soil skeleton,
- the vertical component of shear forces, $T_s^{(v)}$, acting in the overburden soil body along the slip surfaces separating the part of the soil involved in breakout from the surrounding soil medium,
- the vertical component of soil suction forces, $T_u^{(v)}$, resulting from differences in pore fluid pressure above and below the pipeline, caused by an attempted upward movement of the pipeline (quasi-dynamic effect).

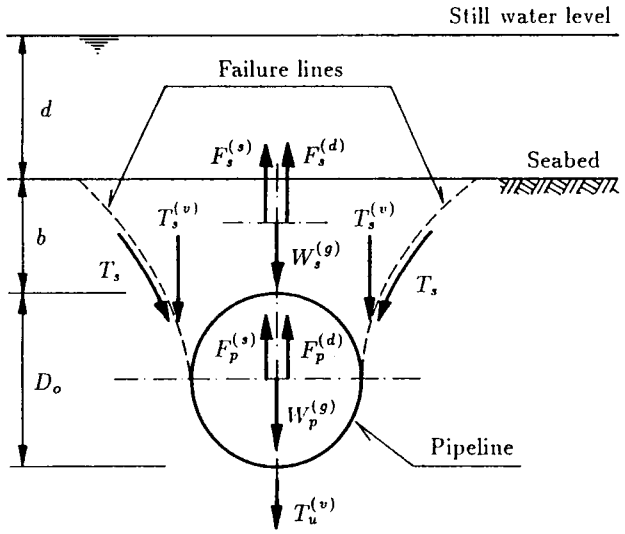

Fig. 9 Component forces assumed for pipeline floatation analysis

All the above mentioned forces have to be understood as forces per unit length of the pipeline. For instability or upward movement of the pipeline, the following condition must be fulfilled (force are positive as shown in Fig. 9):

$$\left(W_p^{(g)} - F_p^{(s)} - F_p^{(d)}\right) + \left(W_s^{(g)} - F_s^{(s)} - F_s^{(d)}\right) + T_s^{(v)} + T_u^{(v)} \leq 0 \qquad (1)$$

which can be also given in terms of the factor of safety against floatation:

$$F_s^{(float)} = \frac{\left(F_p^{(s)} + F_p^{(d)}\right) + \left(F_s^{(s)} + F_s^{(d)}\right)}{W_p^{(g)} + W_s^{(g)} + T_s^{(v)} + T_u^{(v)}} \geq 1 \qquad (2)$$

In the following, the main results of a computational analysis of the pipeline stability with respect to the above mentioned 8 experimental cases of the free-movable pipeline dynamic tests are presented.

4.1 Evaluation of the component forces

Effective weight of the pipeline

The weight of the pipeline, together with its content can be easily evaluated using the following formula:

$$W_p^{(g)} = \frac{\pi}{4}\left\{\left[D_o^2 - (D_o - 2s)^2\right]\gamma_{st} + (D_o - 2s)^2\gamma_c\right\} \qquad (3)$$

where: $W_p^{(g)}$ is the weight of pipeline, D_o is the outside diameter of the pipeline, s is the thickness of the pipeline wall, γ_{st} is the unit weight of the pipe material, and γ_c is the unit weight of the pipeline content.

The buoyancy force (uplift force) consists of hydrostatic and hydrodynamic components, where the later is induced by oscillating water loading (*e.g.*, progressive surface water waves, or vertical oscillations of the water-table as in the present experiments). The hydrostatic component of the uplift force acting on the pipeline is given by the Archimedes law:

$$F_p^{(s)} = \frac{\pi D_o^2}{4}\gamma_w = \pi r_p^2\gamma_w = A_p\gamma_w \qquad (4)$$

where, additionally: $F_p^{(s)}$ is the hydrostatic uplift force acting on the pipeline, γ_w is the unit weight of water, r_p is the outside radius of the pipeline, and A_p is the area of the pipeline cross-section. For the experimental conditions, this force is constant and equal $F_p^{(s)} = 0.0770\,\mathrm{kN/m}$.

For the purpose of the experiments, another formula was used, namely:

$$W_p^{(s)} = W_p^{(g)} - F_p^{(s)} = \frac{\pi D_o^2}{4}(G_p - 1)\gamma_w = \pi r_p^2(G_p - 1)\gamma_w = A_p(G_p - 1)\gamma_w \qquad (5)$$

where, additionally: $W_p^{(s)}$ is the submerged (buoyant) weight of the pipeline, and G_p is the specific gravity of the pipeline.

Assuming $\gamma_w = 9.81\,\mathrm{kN/m^3}$ and $D_o = 0.1\,\mathrm{m}$ (i.e. $r_p = 0.05\,\mathrm{m}$) for the test section of the pipeline, one obtains $W_p^{(s)} = -0.0385$, -0.0231, -0.0077, 0.0, and $0.0385\,\mathrm{kN/m}$ for $G_p = 0.5$, 0.7, 0.9, 1.0, and 1.5, respectively.

Among all the environmental loads usually considered in the design procedure established for submarine pipelines buried in sandy seabed sediments, the wave-induced pore pressure – besides the hydrostatic pressure – plays one of the most important factors. A non-vertical distribution of the wave induced pore pressure with depth is responsible for creating the wave-induced pore pressure gradient which, in turn,

can cause instability of an upper part of the seabed layer, soil liquefaction, and consequently – floatation of the pipeline which normally leads easily to serious failures of submarine pipelines. And even if thete is no soil liquefaction in the close proximity of the pipeline, this is also the case very relevant for the engineering practice. Continuously oscillating water pressure loading induces instantaneously oscillating hydrodynamic seepage forces acting on the pipeline. A vertical component of the resultant seepage force, acting upwards and trying to lift up the pipeline from the seabed, is called the wave-induced uplift force or hydrodynamic uplift force, contrary to the time-independent hydrostatic uplift force simply described by the Archimedes law. The hydrodynamic uplift force has a character of an oscillating force due to also oscillating type of surface water loading and is comparable to the displaced water weight.

The hydrodynamic component of the uplift force, $F_p^{(d)}$ is changing with time, as it was already shown in Fig. 4. For the purpose of the present analysis, some numerical computations were performed in order to find maximum values of the hydrodynamic uplift force, assuming input data representative for the experimental conditions. The results of computations, shown in Fig. 10, illustrate the influence of the depth of burial and soil saturation conditions on the maximum hydrodynamic uplift force. The absolute value of the hydrodynamic uplift force can be found from the following relationship:

$$F_p^{(d)} = \bar{F}_p^{(d)} \times (P_0 D_o) \tag{6}$$

in which:

$$P_0 = \gamma_w A \tag{7}$$

where: $F_p^{(d)}$ is the hydrodynamic uplift force acting on the pipeline, $\bar{F}_p^{(d)}$ is the relative hydrodynamic uplift force, P_0 is the amplitude of hydrodynamic bottom pressure, D_o is the outside diameter of the pipeline, γ_w is the unit weight of water, and A is the amplitude of water head oscillations at sand surface.

From the former laboratory experiments (Magda *et al.*, 1997) it is well-known that the degree of saturation is very high, ranging from $S = 0.992$ to $S = 0.998$. Taking this range into account, using Eqs. (6) and (7) together with the numerical results shown in Fig. 10, and assuming $\gamma_w = 9.81\,\mathrm{kN/m^3}$ and $A = 0.40\,\mathrm{m}$, Tab. 2 gives the proper values of the hydrodynamic uplift force.

Effective weight of soil body involved in breakout

The volume of soil mass involved in breakout depends, in general, on the depth of embedment, $D_b = b + r_p$, and the relative density, D_r. Vesic (1971) reported that shallow anchors fail along the general slip surface as shown in Fig. 11(b). Deep anchors move vertically for a considerable distance producing a failure patern similar to punching shear failure, shown in

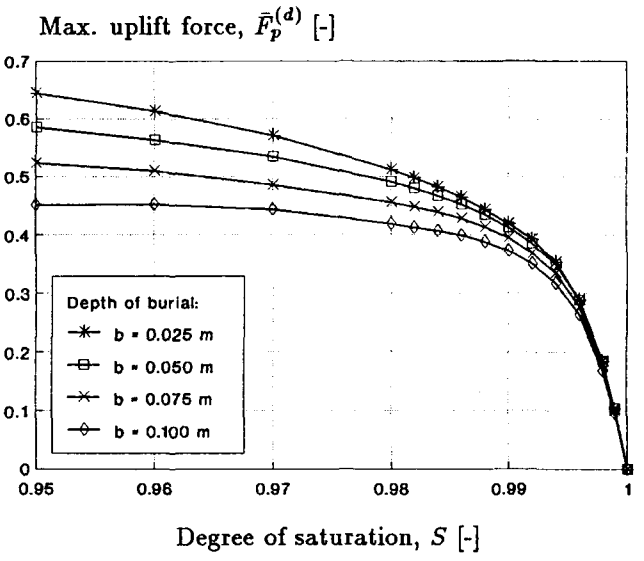

Fig. 10 Maximum hydrodynamic uplift force acting on the pipeline, computed numerically for different soil saturation conditions and depth of burial

Table 2 Maximum hydrodynamic uplift force, $F_p^{(d)}$ [kN/m], acting on the pipeline, for different soil saturation conditions and depths of burial.

Saturation	Depth of burial, b [m]			
S [-]	0.025	0.050	0.075	0.100
0.992	0.1540	0.1508	0.1443	0.1372
0.994	0.1388	0.1367	0.1311	0.1241
0.996	0.1136	0.1129	0.1089	0.1036
0.998	0.0724	0.0720	0.0695	0.0661

Fig. 11(a), and then fail along the general slip surface. Vesic (1971) suggested that the cricital relative depth, D_b/D_o, may increase in sand from 2, for a very loose deposit, to over 10 in a very dense deposit.

For all the cases investigated in the present study $D_b/D_o = 0.75 - 1.5$, which would indicate the type of failure along the general slip surface [see Fig. 11(b)], regardless the relative density of the sand model. Using some simple trigonometric relations, the cross-sectional area of the soil body involved in breakout can be given as:

$$A_s^{(g)} = A_s^{(p)} + 2A_s^{(a)} \tag{8}$$

in which:

$$A_s^{(p)} = 2r_p(b + r_p) - \frac{\pi r_p^2}{2} = 2r_p\left[b + r_p\left(1 - \frac{\pi}{4}\right)\right] \tag{9a}$$

$$A_s^{(a)} = (b + r_p)^2 \frac{2 - \cos\beta - \dfrac{\beta}{\sin\beta}}{2\sin\beta} \tag{9b}$$

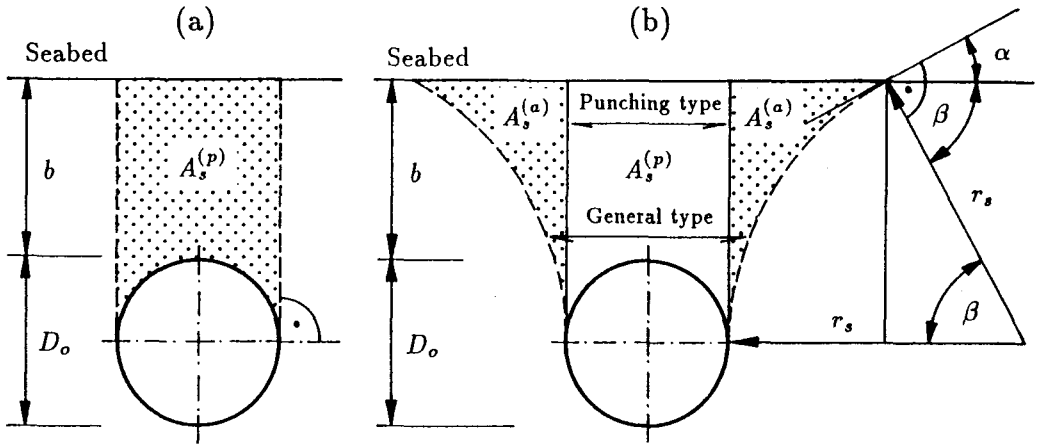

Fig. 11 Theoretical shapes of soil body involved in breakout: (a) punching type of shear failure along vertical lines, (b) general type of shear failure along non-linear lines

in which:

$$\alpha = \frac{\pi}{4} - \frac{\phi}{2} \tag{9c}$$

$$\beta = \frac{\pi}{2} - \alpha = \frac{\pi}{4} + \frac{\phi}{2} \tag{9d}$$

where: $A_s^{(g)}$ is the total cross-sectional area of the soil body involved in the general type of failure, $A_s^{(p)}$ is the cross-sectional area of the soil body involved in the punching type of failure, $A_s^{(a)}$ is the additional cross-sectional area, showing the difference between the punching type and the general type of failure, b is the depth of burial of the pipeline, r_p is the outside radius of the pipeline, and ϕ is the angle of internal friction of the soil.

Table 3 presents a comparison between the component cross-sectional areas of the soil body involved in breakout [$\phi = 35°$ ("Toyoura" standard sand) and $r_p = D_o/2 = 0.05$ m were assumed in the computations].

After assuming the volume involved, the effective weight of the soil mass which accounts for seepage forces has to be evaluated. The effective weight of the soil mass, similar to the uplift force acting on the pipeline, can be divided into hydrostatic and hydrodynamic parts. The weight of the soil can be combined with the hydrostatic component of the uplift force in the following equation:

$$W_s^{(s)} = W_s^{(g)} - F_s^{(s)} = A_s \frac{G_s - 1}{1 + e}\gamma_w = A_s \gamma' \tag{10}$$

where: $W_s^{(s)}$ is the submerged (buoyant) weight of the soil skeleton involved in breakout, $W_s^{(g)}$ is the weight of the soil skeleton involved in breakout, $F_s^{(s)}$ is the hydrostatic component of the uplift force acting on the soil body involved in breakout, A_s is the total cross-sectional area of the soil body involved in breakout, G_s is the specific gravity of the soil skeleton, e is the void ratio, γ' is the buoyant (submerged) unit weight of the soil, and γ_w is the unit weight of water.

During the falling state of water-table oscillating loading, there are also seepage forces acting in the soil body involved, contributing thereby to minimize the effective weight of the soil body involved in breakout. Considering a hydrodynamically-induced vertical component of the resultant seepage force, responsible for creating a vertical hydrodynamic pore pressure gradient, one can write:

$$F_s^{(d)} = A_s \gamma_w i_d \tag{11}$$

where: $F_s^{(d)}$ is the hydrodynamic component of the uplift force acting on the soil body involved in breakout, A_s is the cross-sectional area of the soil body involved in breakout, γ_w is the unit weight of water, and i_d is the vertical (positive as upward) seepage gradient.

Table 3 Comparison of cross-sectional areas of the soil body involved in breakout.

b [m]	$A_s^{(p)}$ [m^2]	$2A_s^{(a)}$ [m^2]	$A_s^{(g)}$ [m^2]	$r_A = A_s^{(p)}/A_s^{(g)}$ [%]
0.025	3.573×10^{-3}	1.956×10^{-3}	5.529×10^{-3}	64.6
0.050	6.073×10^{-3}	3.478×10^{-3}	9.551×10^{-3}	63.9
0.075	8.573×10^{-3}	5.434×10^{-3}	14.007×10^{-3}	61.2
0.100	11.073×10^{-3}	7.825×10^{-3}	18.898×10^{-3}	58.6

Putting the last two equations together, the effective weight of the soil body involved in breakout is:

$$W_s^{(e)} = W_s^{(s)} - F_s^{(d)} = A_s\gamma' - A_s\gamma_w i_d$$
$$= A_s(\gamma' - \gamma_w i_d) = A_s\gamma'' \qquad (12)$$

where, additionally: $W_s^{(e)}$ is the effective weight of the soil body involved in breakout, γ'' is the apparent unit weight of the soil body involved in breakout.

Of course, Eq. (12) makes sense as long as $W_s^{(e)} \geq 0$; if $W_s^{(e)} < 0$, a 'quick sand' or soil liquefaction condition is reached and $W_s^{(e)}$ has to be set to zero in the global analysis of the pipeline vertical stability.

For a definition of the average hydrodynamic vertical seepage gradient, Fig. 12 can be used. And thus:

$$i_d = -\frac{h_{z=0} - h_{z=b}}{b} \qquad (13)$$

where: i_d is the average hydrodynamic vertical seepage gradient (upward to be positive), b is the depth of burial of the pipeline, $h_{z=0}$ is the hydrodynamic pore pressure (unit: m of water head) at the sand surface, and $h_{z=b}$ is the hydrodynamic pore pressure (unit: m of water head) at the top of the pipeline.

Based on the results of the finite-element numerical 2D-analysis (Magda, 1996, 1997) as for the computation of the hydrodynamic uplift force acting on the pipeline, the effective weight of the soil body involved in breakout was computed and presented in Tab. 4 (punching type of failure; $W_s^{(ep)}$) and Tab. 5 (general type of failure; $W_s^{(eg)}$), for different depths of burial of the pipeline tested in the small-scale experiments. The numerical results for the hydrodynamic pore pressure gradient were obtained assuming the soil saturation to be $S = 0.996$ (Magda *et al.*, 1998). Figure 13 illustrates the finite-element mesh from the pipeline vicinity, used in the numerical modelling of the governing problem.

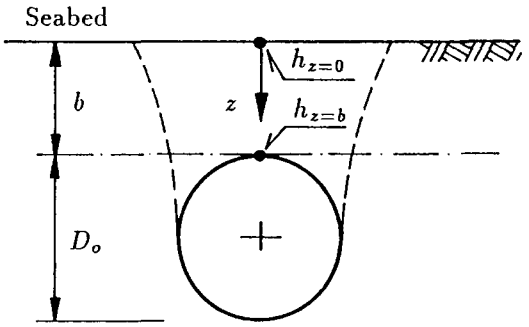

Fig. 12 Definition of the average hydrodynamic vertical seepage gradient

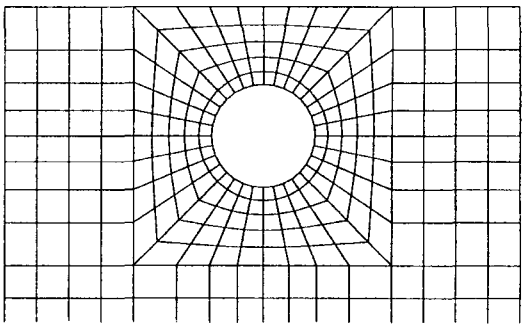

Fig. 13 Finite-element mesh (pipeline vicinity) used in numerical modelling

Table 4 Effective weight of the soil body involved in breakout, $W_s^{(ep)}$, in punching type of failure ($S = 0.996$).

b [m]	$W_s^{(sp)}$ [kN/m]	i_d [-]	$F_s^{(dp)}$ [kN/m]	$W_s^{(ep)}$ [kN/m]
0.025	3.4622×10^{-2}	0.1778	0.6232×10^{-2}	2.8390×10^{-2}
0.050	5.8847×10^{-2}	0.3836	2.2853×10^{-2}	3.5994×10^{-2}
0.075	8.3072×10^{-2}	0.4966	4.1765×10^{-2}	4.1307×10^{-2}
0.100	10.7297×10^{-2}	0.5607	6.0907×10^{-2}	4.6390×10^{-2}

Table 5 Effective weight of the soil body involved in breakout, $W_s^{(eg)}$, in general type of failure ($S = 0.996$).

b [m]	$W_s^{(sg)}$ [kN/m]	i_d [-]	$F_s^{(dg)}$ [kN/m]	$W_s^{(eg)}$ [kN/m]
0.025	5.3576×10^{-2}	0.1778	0.9644×10^{-2}	4.3932×10^{-2}
0.050	9.2549×10^{-2}	0.3836	3.5942×10^{-2}	5.6607×10^{-2}
0.075	13.5728×10^{-2}	0.4966	6.8237×10^{-2}	6.7491×10^{-2}
0.100	18.3122×10^{-2}	0.5607	10.3948×10^{-2}	7.9174×10^{-2}

Shear resistance vertical component

An analytical approach to the vertical component of the shearing resistance was proposed by Vesic (1971) who compared this problem with the expansion of cavities near the surface of a semi-infinite plastic solid mass. Phillips *et al.* (1979) carried out extensive experiments in order to study the stability of pipelines in sandy soils, and concluded that Vesic's (1971) theory overestimates the soil resistance because the theory did not consider wave-induced pore pressures and the corresponding reduction in effective stresses.

Taking the above into account, the numerical results (based on the finite-element modelling) were used in the present study to estimate the effective shear stress in the pipeline vicinity, due to oscillating water-table loading. But first, the shear stress under hydrostatic conditions needs to be estimated and checked. As before, the two different schemes of the shear failure are assumed for the comparison analysis:

- punching type of shear failure [Fig. 14(a)],
- general type of shear failure [Fig. 14(b)].

The shear stress acting along the vertical failure lines in the soil mass above the pipeline [punching type of failure; see Fig. 14(a)] can be expressed as:

$$\tau_s^{(p)} = \tau_s^{(vp)} = \sigma_x \tan\phi \tag{14}$$

where: $\tau_s^{(p)}$ is the shear stress in the punching type of failure, $\tau_s^{(vp)}$ is the vertical component of the shear stress in the punching type of failure, σ_x is the horizontal normal stress, and ϕ is the angle of internal friction of the soil.

The horizontal normal stress is simply related with the vertical normal stress in the following equation:

$$\sigma_x = K_0\sigma_z = \frac{\nu}{1-\nu}\sigma_z \tag{15}$$

where, additionally: σ_z is the vertical normal stress, K_0 is the coefficient of lateral pressure at-rest, and ν is the Poisson ratio.

The vertical normal stress in the soil is given by:

$$\sigma_z = \gamma' z \tag{16}$$

where: γ' is the submerged unit weight of soil, and z is the depth in the soil.

In order to be more correct, due to the presence of hydrodynamic loading, the normal stresses in the governing problem have to be treated in terms of effective stresses. Here, at least two methods exist to assess the value thereof, namely:

$$\sigma_z^{(e)} = \sigma_z - p \tag{17a}$$

$$\sigma_z^{(e)} = \sigma_z - \sigma_z' \tag{17b}$$

where: $\sigma_z^{(e)}$ is the effective vertical normal stress, σ_z is the vertical normal stress (under hydrostatic conditions), p is the hydrodynamic pore pressure, and σ_z' is the vertical normal stress induced by vertical water-table oscillations.

For the purpose of the present analysis, the first definition [see Eq. (17a)] will be used in the following. Therefore, by combining Eqs. (14), (15), (16), and (17a), one obtains:

$$\tau_s^{(vp)} = \frac{\nu}{1-\nu}(\gamma' z - p)\tan\phi \tag{18}$$

The resultant shear force, acting on both sides of the soil body involved in breakout of the punching type, can be obtained by the following simple integration:

$$T_s^{(vp)} = 2\int_0^{b+r_p} \tau_s^{(vp)}\, dz = 2\frac{\nu}{1-\nu}\tan\phi \int_0^{b+r_p} (\gamma' z - p)\, dz \tag{19}$$

where, additionally: $T_s^{(vp)}$ is the vertical component of the resultant shear force, b is the depth of burial of the pipeline, and r_p is the outside radius of the pipeline.

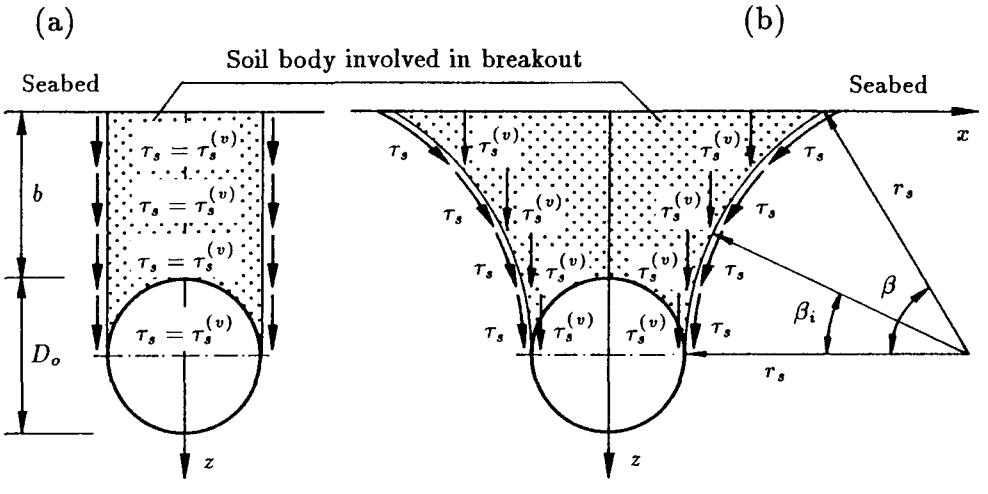

Fig. 14 Definition of shear forces acting along failure lines: (a) punching type of shear failure, (b) general type of shear failure

The term $(\gamma' z - p)$ accounts for the presence of hydrodynamic loading in the definition of normal soil stresses which have to be treated in terms of effective stresses. If the hydrodynamic pore pressure function, p, is known, the above integral can be computed. However, for the purpose of comparison with the static pull-out tests, $p = 0$ can be assumed and the solution to the above integral can be found analytically. And thus, the resultant shear force, acting on both sides of the soil body involved in breakout induced by a static pull-out force, is given by the following expression:

$$T_s^{(vp)} = (b + r_p)^2 \frac{\nu}{1-\nu} \gamma' \tan\phi \tag{20}$$

The shear stress acting along the general (non-linear) failure line in the soil mass above the pipeline [see Fig. 14(b)] is a little bit more difficult to be defined analytically. First of all, a relation between the shear stresses, uniformly distributed along the slip surfaces appearing in the punching and general type of failure must be presented:

$$\tau_s^{(vg)} = \tau_s^{(g)} \cos\beta_i \tag{21}$$

where: $\tau_s^{(vg)}$ is the vertical component of the shear stress acting along the slip surface in the general type of failure, $\tau_s^{(g)}$ is the shear stress acting along the slip surface in the general type of failure, and β_i is the angle describing the position of computational point located on the slip surface.

Taking into account that the shear failure is non-linear, being an arc of the circle of radius [see Fig. 14(b)]:

$$r_s = \frac{b + r_p}{\sin\beta} \tag{22}$$

the vertical component of the resultant shear force in the general type of failure, analogically to the former case, can be found from the following expression:

$$T_s^{(vg)} = 2\int_0^{l_s} \tau_s^{(vg)}\, dl = 2\frac{\nu}{1-\nu}\tan\phi \int_0^{l_s} (\gamma' z - p)\cos\beta_i\, dl \tag{23}$$

in which:

$$l_s = r_s\beta = \frac{b + r_p}{\sin\beta}\beta \tag{24}$$

As before, the knowledge of p-function is required in order to find a solution to the integral in Eq. (23). But again, for comparison with the results of the static pull-out tests, the above integral can be simplified assuming $p = 0$. Additionally, because the depth, z, and the length of the arc, l, are the functions of the angle, β_i, the relations between these parameters are required to proceed with the derivation.

And thus:

$$z = (b + r_p)\left(1 - \frac{\sin\beta_i}{\sin\beta}\right) \tag{25}$$

and

$$l = r_s\beta_i = \frac{b + r_p}{\sin\beta}\beta_i \tag{26}$$

where: z is the vertical coordinate (depth in the soil), b is the depth of burial, $r_p = D_o/2$ is the outside radius of the pipeline, β_i is the angle describing the position of computational point located on the slip surface, $\beta = \pi/4 + \phi/2$ is the angular length of the general slip surface, and l is the length of the failure arc-line.

Differentiating Eq. (26), one has:

$$dl = \frac{b + r_p}{\sin\beta} d\beta_i \tag{27}$$

and, replacing the variables of integration from l into β_i, Eq. (23) can be rewritten into the following form:

$$T_s^{(vg)} = 2\frac{\nu}{1-\nu}\gamma' \tan\phi \int_0^{\beta} (b + r_p)\left(1 - \frac{\sin\beta_i}{\sin\beta}\right)\cos\beta_i \frac{b + r_p}{\sin\beta}\, d\beta_i \tag{28}$$

Solving the above integral analytically, one obtains:

$$\int_0^{\beta} (b + r_p)\left(1 - \frac{\sin\beta_i}{\sin\beta}\right)\cos\beta_i \frac{b + r_p}{\sin\beta}\, d\beta_i = \frac{(b + r_p)^2}{2} \tag{29}$$

Introducing the result of the above integral into Eq. (28), the vertical component of the resultant shear force, acting along the general failure line, is given as:

$$T_s^{(vg)} = (b + r_p)^2 \frac{\nu}{1-\nu}\gamma' \tan\phi \tag{30}$$

where: $T_s^{(vg)}$ is the vertical component of the resultant shear force acting along the general failure line, ν is the Poisson ratio of the soil, γ' is the submerged unit weight of the soil, ϕ is the angle of internal friction of the soil, b is the depth of burial of the pipeline, and r_p is the outside radius of the pipeline.

Comparing Eq. (30) with Eq. (20), it becomes surprisingly obvious that the shear resistance force (its vertical component) associated with the general slip surface [non-linear arc-shaped line; see Fig. 14(b)] does not differ from the shear resistance force related to the punching type of failure line [vertical line; see Fig. 14(a)]. The solution obtained for the arc-shaped slip surface is independent of angle β.

Table 6 shows the values of the shear resistance force computed for either the punching type or general type of failure line, and for different cases of the depth of burial. The results presented are obtained for the case of the static pull-out force (*i.e.*, assuming $p = 0$) and $\nu = 0.4$ and $\phi = 35°$.

Table 6 Vertival component of the resultant shear resistance force.

b [m]	$T_s^{(vp)} = T_s^{(vg)}$ [kN/m]
0.025	2.544×10^{-2}
0.050	4.523×10^{-2}
0.075	7.068×10^{-2}
0.100	10.178×10^{-2}

The comparison of the results (presented in Tab. 4, Tab. 5, and Tab. 6) reveals that the shear force is pretty much comparable with the static submerged weight of the soil body involved in breakout, $W_s^{(s)}$. In case of the punching type of failure, the shear force is equal to 90.2 %, 94.3 %, 104.4 %, and 116.4 % of $W_s^{(s)}$, for the depth of burial $b = 0.025$, 0.050, 0.075, and 0.100 m, respectively. In case of the general type of failure, this ratio is smaller, due to larger volumes of the soil body involved in breakout, where the shear force is equal to 58.3 %, 60.0 %, 63.9 %, and 68.2 % of $W_s^{(s)}$, respectively.

4.2 Evaluation of global stability condition

Hydrostatic case ($p = 0$)

Having all the static forces defined, it becomes possible to compare the pull-out forces computed analytically and measured experimentally in the static pull-out tests. The static pull-out force can be defined as [see Eq. (1)]:

$$W^{(s)} = \left(W_p^{(g)} - F_p^{(s)}\right) + \left(W_s^{(g)} - F_s^{(s)}\right) + T_s^{(v)} = W_p^{(s)} + W_s^{(s)} + T_s^{(v)} \tag{31}$$

where: $W^{(s)}$ is the static pull-out force, $W_p^{(g)}$ is the weight of the pipeline, $F_p^{(s)}$ is the hydrostatic uplift force acting on the pipeline, $W_p^{(s)}$ is the submerged (buoyant) weight of the pipeline, $W_s^{(g)}$ is the weight of the soil body involved in breakout, $F_s^{(s)}$ is the hydrostatic uplift force acting on the soil skeleton involved in breakout, $W_s^{(s)}$ is the submerged (buoyant) weight of the soil body involved in breakout, $T_s^{(v)}$ is the vertical component of the shear resistant force acting along the failure lines, and $T_u^{(v)}$ is the vertical component of the resultant suction force.

In case of the static analysis, $T_u^{(v)}$ appearing in the stability equation [see Eqs. (1) and (2)] is set to zero. Based on the previously presented results, the static pull-out force, computed analytically, is given in Tab. 7 for the punching type of failure, and Tab. 8

Table 7 Static pull-out force, $W^{(sp)}$ [kN/m], acting on buried pipeline and leading to the punching type of failure (analytical solution).

Spec. gravity of pipeline	Depth of burial, b [m]			
G_p [-]	0.025	0.050	0.075	0.100
0.5	2.156×10^{-2}	6.558×10^{-2}	11.525×10^{-2}	17.058×10^{-2}
0.7	3.696×10^{-2}	8.098×10^{-2}	13.065×10^{-2}	18.598×10^{-2}
0.9	5.236×10^{-2}	9.638×10^{-2}	14.605×10^{-2}	20.138×10^{-2}
1.0	6.006×10^{-2}	10.408×10^{-2}	15.375×10^{-2}	20.908×10^{-2}
1.5	9.856×10^{-2}	14.258×10^{-2}	19.225×10^{-2}	24.758×10^{-2}

Table 8 Static pull-out force, $W^{(sg)}$ [kN/m], acting on buried pipeline and leading to the general type of failure (analytical solution).

Spec. gravity of pipeline	Depth of burial, b [m]			
G_p [-]	0.025	0.050	0.075	0.100
0.5	4.052×10^{-2}	9.928×10^{-2}	16.791×10^{-2}	24.640×10^{-2}
0.7	5.592×10^{-2}	11.468×10^{-2}	18.331×10^{-2}	26.180×10^{-2}
0.9	7.132×10^{-2}	13.008×10^{-2}	19.871×10^{-2}	27.720×10^{-2}
1.0	7.902×10^{-2}	13.778×10^{-2}	20.641×10^{-2}	28.490×10^{-2}
1.5	11.752×10^{-2}	17.628×10^{-2}	24.491×10^{-2}	32.340×10^{-2}

Table 9 Comparison of pull-out forces (assuming $G_p = 1.0$) measured experimentally, $W^{(st)}$, and computed analytically: $W^{(sp)}$ (punching type of failure), $W^{(sg)}$ (general type of failure).

b [m]	$M^{(st)}$ [kg]	$W^{(st)}$ [kN/m]	$W^{(st)}/W^{(sp)}$ [-]	$W^{(st)}/W^{(sg)}$ [-]
0.025	3.75	9.681×10^{-2}	1.61	1.23
0.050	6.80	17.555×10^{-2}	1.69	1.27
0.075	9.35	24.138×10^{-2}	1.57	1.17
0.100	15.34	39.601×10^{-2}	1.97	1.39

for the general (arc-shaped) type of failure, obtained for different values of the specific gravity of pipeline, G_p, and the depth of burial, b.

Table 9 presents the experimental results of the static pull-out force, $W^{(st)}$, and compares them with the theoretical values obtained for the punching type of failure ($W^{(sp)}$, see Tab. 7) and the general type of failure ($W^{(sg)}$, see Tab. 8). The static pull-out force (weight) was found from the following expression:

$$W^{(st)} = \frac{M^{(st)}}{L_p} \frac{g}{1.000} \tag{32}$$

where: $W^{(st)}$ is the static pull-out force, $M^{(st)}$ is the static pull-out mass, g is the acceleration due to gravity, and L_p is the length of the pipeline test section.

The static pull-out tests were performed for only one value of the specific gravity of the pipeline $G_p = 1.0$. In the computations, $g = 9.81\,\mathrm{m/s^2}$ and $L_p = 0.38\,\mathrm{m}$ were assumed.

The above comparison reveals that the general type of shear failure approximates better the measured values of the static pull-out force than the punching type of failure. The analytical solution obtained for the general (arc-shaped) type of failure is more or less 20 % higher than the experimental values. However, it has to be noted that the static pull-out tests had a character of 3D-modelling where the both ends of the pipeline test section create an additional shear resistance against the upward movement of the pipeline. Roughly estimating, the shear resistance induced by the ends of the pipeline is $D_o/L_p = 0.1/0.38 \simeq 26\,\%$ of the shear resistance activated along the pipeline. Taking it into account, the analytical solution for the general type of failure stays in a very good accordance with the measured values, and only the case of $b = 0.1\,\mathrm{m}$ shows that the experimental value is still approx. 20 % higher than the theoretical one.

It is rather difficult to judge about the type of shear failure observed in the static pull-out tests (see Photo 1). In fact, two different slip lines can be distinguished where the first one indicates the punching type of failure and the second one indicates much larger area of the soil involved in breakout. The main problem is that it is extremely difficult to observe the situation that happens exactly at the initial phase of the shear failure where the pull-out force reaches its maximum. When the initial time-point is overcome, the sand movement in the pipeline vicinity becomes more complex, i.e. some parts moves upward together with the pipeline, and some others 'flows' downward filling out empty spaces caused by the upward movement of the pipeline.

The computation of the pull-out force can be also performed using the so-called cavity breakout factor, F_q, given by Vesic (1971), depending on the shape and relative depth of the cavity as well as on the angle of internal friction. The factor F_q can be used directly (from appropriate tables) for embadded spheres or embadded horizontal cylinders. Assuming $\phi = 35°$, $r_p = D_o/2 = 0.05\,\mathrm{m}$, and using linear approximation between the values given in the table, one can easily compute the cavity breakout factor (Tab. 10).

Table 10 Cavity breakout factor, F_q, for the test conditions.

b [m]	$D_b = b + r_p$ [m]	F_q [-]
0.025	0.075	0.8075
0.050	0.100	1.1350
0.075	0.125	1.3325
0.100	0.150	1.5300

For the calm sea condition (*i.e.*, $p = 0$; no seepage forces), Vesic (1971) suggests the following expression:

$$\frac{W_s^{(s)} + T_s^{(v)}}{D_o} = \gamma' D_b F_q \tag{33}$$

where: $W^{(s)}$ is the static pull-out force, $T_s^{(v)}$ is the vertical component of the shear resistance force acting along the failure lines, D_o is the outside diameter of the pipeline, γ' is the submerged (buoyant) unit weight of water, D_b is the depth of the pipeline centre, and F_q is the cavity breakout factor.

Rearranging Eq. (33), one has:

$$W_s^{(F)} = \gamma' D_b F_q D_o \tag{34}$$

Table 11 Comparison between the pull-out forces (assuming $G_p = 1.0$), computed analytically [$W_s^{(fp)}$ (punching type of failure), and $W_s^{(fg)}$ (general type of failure)], and using the cavity breakout factor, $W_s^{(F)}$.

b [m]	$W_s^{(fp)}$ [kN/m]	$W_s^{(fg)}$ [kN/m]	$W_s^{(F)}$ [kN/m]
0.025	6.006×10^{-2}	7.902×10^{-2}	5.869×10^{-2}
0.050	10.408×10^{-2}	13.778×10^{-2}	10.998×10^{-2}
0.075	15.375×10^{-2}	20.641×10^{-2}	16.140×10^{-2}
0.100	20.138×10^{-2}	28.490×10^{-2}	22.239×10^{-2}

Table 11 illustrates the comparison between the pull-out forces, excluding the influence of the submerged weight of the pipeline (*i.e.*, $W_p^{(s)} = 0$, which is adequate to the case $G_p = 1.0$). The pull-out force, computed using the cavity breakout factor, is denoted by $W_s^{(F)}$, whereas the pull-out force, computed using the formerly derived formulas, is denoted by $W_s^{(fp)} = W_s^{(sp)} + T_s^{(vp)}$ (punching type of failure), and $W_s^{(fg)} = W_s^{(sg)} + T_s^{(vg)}$ (general type of failure).

The results of the pull-out force given in Tab. 11 indicate clearly that the computation with the cavity breakout factor are much more closer to the analytical solution obtained for the punching type of failure than for the general type of failure, although the depth of embedment, $D_b = 0.075 - 0.15$ would rather indicate, according to Vesic (1971), the general type of failure.

Hydrodynamic case ($p \neq 0$)

Based on the knowledge of all static and hydrodynamic forces acting on the pipeline and the soil body involved in breakout, it becomes possible to analyse the global stability condition against floatation of the pipeline buried in seabed sediments and loaded by surface water oscillations. The resultant vertical force can be given as [see Eq. (1)]:

$$\begin{aligned} W^{(d)} &= \left(W_p^{(g)} - F_p^{(s)} - F_p^{(d)}\right) + \left(W_s^{(g)} - F_s^{(s)} - F_s^{(d)}\right) \\ &\quad + T_s^{(v)} + T_u^{(v)} \\ &= \left(W_p^{(s)} - F_p^{(d)}\right) + \left(W_s^{(s)} - F_s^{(d)}\right) \\ &\quad + T_s^{(v)} + T_u^{(v)} \end{aligned} \tag{35}$$

where: $W^{(d)}$ is the dynamic resultant vertical force, $W_p^{(g)}$ is the weight of the pipeline, $F_p^{(s)}$ is the hydrostatic uplift force acting on the pipeline, $F_p^{(d)}$ is the hydrodynamic uplift force acting on the pipeline, $W_p^{(s)}$ is the submerged (buoyant) weight of the pipeline, $W_s^{(g)}$ is the weight of the soil body involved in breakout, $F_s^{(s)}$ is the hydrostatic uplift force acting on the soil skeleton involved in breakout, $F_s^{(d)}$ is the hydrodynamic uplift force (seepage force) acting on the soil skeleton involved in breakout, $W_s^{(s)}$ is the submerged (buoyant) weight of the soil body involved in breakout, $T_s^{(v)}$ is the vertical component of the shear resistant force acting along the failure lines, and $T_u^{(v)}$ is the vertical component of the resultant suction force.

In the static pull-out tests, it was quite reasonable to assume $T_u^{(v)} = 0$ because of a very slow, gradual application of the force that induced an extremely slow and small upward movement of the pipeline (*i.e.*, static case). In the pipeline floatation tests, however, the additional hydrodynamic forces appear, contributing thereby to a different pattern of the pipeline vertical movement. The hydrodynamic pore pressure field around the pipeline is responsible for the pipeline vertical movement, and not *vice versa*. Therefore, it seems reasonable to assume that $T_u^{(v)} \simeq 0$ also for all the hydrodynamic tests on the pipeline floatation. The additional pore pressure increments induced at the top and at the bottom of the pipeline, due to the vertical movement of the pipeline (dynamic effect), are believed to be relatively small compared with the hydrodynamic pore pressure induced by water loading.

Based on the previously presented results of the static pull-out force computed analytically (see Tab. 7, for the punching type of failure, and Tab. 8, for the general type of failure), as well as the hydrodynamic uplift force ($S = 0.996$) acting on the pipeline (see Tab. 2) and the hydrodynamic seepage force ($S = 0.996$) acting on the soil body involved in breakout (see Tab. 4, for the punching type of failure, and Tab. 5, for the general type of failure), the global stability against floatation was computed and illustrated in Tab. 12 (punching type of failure), and Tab. 13 (general type of failure). Performing some preliminary computations, it was found that the hydrodynamic pore pressure contributes to the reduction of the vertical component of the resultant shear resistance force by approx. 20 %.

The last two figures illustrate the analytical solution of the dynamic resultant vertical force, $W^{(d)}$, as a function of the depth of burial (Fig. 15) and the specific gravity of pipeline (Fig. 16). Here, only these results are put together which are adequate to the conditions modelled in the dynamic pipeline floatation tests.

Table 12 Dynamic resultant vertical force, $W^{(dp)}$ [kN/m], in the global stability analysis (punching type of failure; $S = 0.996$).

Spec. gravity of pipeline	Depth of burial, b [m]			
G_p [-]	0.025	0.050	0.075	0.100
0.5	-10.336×10^{-2}	-7.922×10^{-2}	-4.956×10^{-2}	-1.429×10^{-2}
0.7	-8.796×10^{-2}	-6.382×10^{-2}	-3.416×10^{-2}	0.111×10^{-2}
0.9	-7.256×10^{-2}	-4.842×10^{-2}	-1.876×10^{-2}	1.651×10^{-2}
1.0	-6.486×10^{-2}	-4.072×10^{-2}	-1.105×10^{-2}	2.421×10^{-2}
1.5	-2.636×10^{-2}	-0.222×10^{-2}	2.745×10^{-2}	6.271×10^{-2}

Table 13 Dynamic resultant vertical force, $W^{(dg)}$ [kN/m], in the global stability analysis (general type of failure; $S = 0.996$).

Spec. gravity of pipeline	Depth of burial, b [m]			
G_p [-]	0.025	0.050	0.075	0.100
0.5	-8.781×10^{-2}	-5.861×10^{-2}	-2.337×10^{-2}	1.849×10^{-2}
0.7	-7.241×10^{-2}	-4.321×10^{-2}	-0.797×10^{-2}	3.389×10^{-2}
0.9	-5.701×10^{-2}	-2.781×10^{-2}	0.743×10^{-2}	4.929×10^{-2}
1.0	-4.931×10^{-2}	-2.011×10^{-2}	1.513×10^{-2}	5.699×10^{-2}
1.5	0.063×10^{-2}	1.839×10^{-2}	5.363×10^{-2}	9.549×10^{-2}

Comparison of the analytically obtained results (see Figs. 15 and 16) with the experimentally observed behaviour of the pipeline upward movement (see Figs. 7 and 8, respectively) has proved (in a global way) the correctness of estimation of all the component forces that have to be taken into account in the pipeline stability analysis against floatation.

The change in the pipeline stability (floatation) conditions, observed between Case 8 (pipeline stability) and all the other cases of the laboratory experiments (pipeline instability) has been reflected in the analytically performed stability analysis for the general (arc-shaped) type of shear failure.

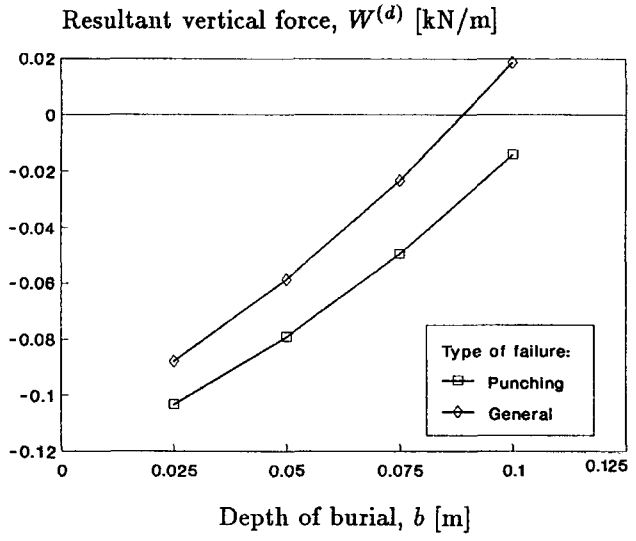

Fig. 15 Influence of the depth of burial on the dynamic resultant vertical force in the global pipeline stability analysis ($G_p = 0.5$)

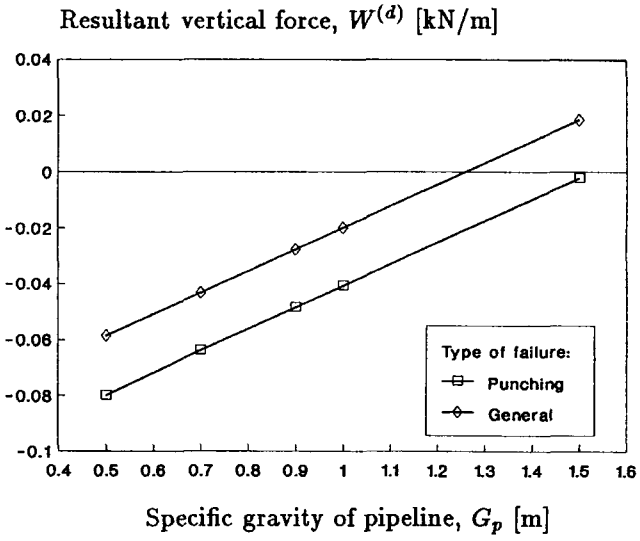

Fig. 16 Influence of the specific gravity of pipeline on the dynamic resultant vertical force in the global pipeline stability analysis ($b = 0.05$ m)

5 CONCLUSIONS

The problem of stability (floatation) of the submarine pipeline buried in sandy seabed sediments has been investigated experimentally (small-scale modelling) and theoretically. The influence of the hydrodynamic loading, induced by cyclically oscillating vertical movements of the surface water-table, has been incorporated into the forces appearing in the global stability condition.

From the two different schemes of the shear failure of the soil covering the pipeline, the general (arc-shaped) type of failure seems to create a better approximation which has been proved by the results of the static pull-out tests and the comparison between the results of the pipeline floatation dynamic tests and the theoretical modelling of the governing phenomenon. The change in the pipeline stability (floatation) conditions, observed between Case 8 (pipeline stability) and all the other cases of the laboratory experiments (pipeline instability) has been reflected in the analytically/numerically performed stability analysis for the general (arc-shaped) type of shear failure.

The main formula [see Eq. (1)], used for assessing the pipeline vertical stability has to be understood as the condition evaluating the potential of pipeline floatation. The resulting hydrodynamic vertical force has an oscillating character, contributing (if the instability condition is fulfilled) to the pipeline instability only within a ceratain time of activation which is a fraction of each period of continuous water loading oscillations. The following behaviour is expected, namely: the longer the time of activation and the amplitude of the hydrodynamic vertical force the shorter the global time leading to floatation of the pipeline. Continuous oscillations of the resultant hydrodynamic vertical force can induce (if the instability condition is fulfilled) a stepwise upward displacement of the pipeline which is hard to be observed after each of oscillations. Therefore, future studies should be directed towards a better explanation of the pipeline floatation phenomenon as a function of global time in macro-scale (*i.e.*, after a certain number of loading cycles) rather than in micro-scale (*i.e.*, within each loading cycle).

In the above presented analysis, the water-table vertical oscillations were considered as a type of water loading. Such treatment was mainly forced by the small-scale of the laboratory experiments performed. However, for practical reasons, the pipeline stability analysis should be, and can be, very easily converted to be able to take into account real water loading conditions formed by progressive surface waves. In general, it is expected to have no significant difference in the results of application of these two types of water loading; the water-table loading can be very often successfully treated as quasi-wave loading because both the pipeline diameter and the depth of burial are much smaller compared with the wavelength. Assuming the real water loading conditions (*i.e.*, progressive surface wave), the findings given by Magda (1997) can be applied, where the maximum hydrodynamic uplift force acting on a submarine pipeline buried in seabed sediments is related to the optimum value of the degree of saturation.

ACKNOWLEDGEMENT

This work is a result of a joined research between the Department of Environmental and Civil Engineering, Okayama University and Marine Civil Engineering Department, Technical University of Gdansk, in the period of November 1988. This research was financially supported by the YAKUMO Foundation, Okayama, Japan and in part by the Grant-in-Aid for Scientific Research (c) of Japan Society for the Promotion of Science (Grant No. 11650529-00, head of researcher : Dr. Shiro Maeno). The Authors gratefully acknowledge these financial support.

REFERENCES

Bobby, W., Arockiasamy, M., Haldar, A.K. (1979). Finite element analysis of pipe-soil-wave interaction. *Proc. of the 2nd International Conference on Behaviour of Off-Shore Structures (BOSS)*, London, England, 28-31 August 1979, Paper No. 39, pp. 503-506.

Cheng, A.H.D., Liu, P.L.-F. (1986). Seepage force on a pipeline buried in a poro-elastic seabed under wave loading. *Applied Ocean Research*, 8(1), pp. 22-32.

Dursthoff, W., Mazurkiewicz, B. (1985). Problems related to subsea pipeline-seabed interaction. *Mitteilungen des Franzius-Instituts für Wasserbau und Küsteningenieurwesen der Universität Hannover*, 61, pp. 176-238.

Maeno, S., Magda, W., Nago, H. (1997). Wave-induced hydrodynamic force acting on a buried submarine pipeline. *Proc. of Coastal Engineering, JSCE*, Vol. 44, No. 2, (in Japanese), pp. 796-800.

Magda, W. (1992). Wave-induced pore water pressure acting on a buried submarine pipeline. *Proc. of the 23rd International Conference on Coastal Engineering (ICCE'92)*, Venice, Italy, 4-9 October 1992, pp. 3135-3148.

Magda, W. (1996). Wave-induced uplift force acting on a submarine buried pipeline. Finite-element formulation and verification computations. *Computers and Geotechnics*, Vol. 19, No. 1, pp. 47-73.

Magda, W. (1997). Wave-induced uplift force on a submarine pipeline buried in a compressible seabed. *Ocean Engineering*, Vol. 24, No. 6, pp. 551-576.

Magda, W. (1998). *Wave-Induced Pore-Pressure Distribution In Sandy Seabed Sediments.* Ph.D. dissertation, Marine Civil Engineering Department, Technical University of Gdansk, Gdansk, Poland.

Magda, W., Maeno, S., Nago, H. (1998). Wave-induced pore-pressure response on a submarine pipeline buried in seabed sediments – experiment and numerical verification. *The Journal of the Faculty of Environmental Science and Technology, Okayama University*, Vol. 3, No. 1, January 1998, pp. 75-95.

McDougal, W.G., Davidson, S.H., Monkmeyer, P.L., Sollit, C.K. (1988). Wave-induced forces on buried pipelines. *Journal of Waterway, Port, Coastal and Ocean Engineering*, ASCE, 114(2), pp. 220-236.

Monkmeyer, P.L., Mantovani, P., Vincent, H. (1983). Wave-induced seepage effects on a buried pipeline. *Proc. of the Coastal Structures '83 Conference*, pp. 519-531.

Nyman, K.J. (1984). Soil response against oblique motion of pipes. *Journal of Transportation Engineering, ASCE*, Vol. 110, No. 2, pp. 190-201.

Phillips, B.A., Ghazzaly, O.I., Kalajian, E.H. (1979). Stability of pipeline in sand under wave pressure. *Proc. of the Speciality Conference 'Civil Engineering in the Ocean IV'*, San Francisco, pp. 122-136.

Pranesh, M.R., Raghava Rao, M. (1997). Seabed thickness–wave–buried pipeline interaction. *Proc. of Offshore Mechanics and Arctic Engineering Conference (OMAE)*, Vol. V, Pipeline Technology, pp. 163-175.

Siddharthan, R., Norris, G.M. (1993). Analysis of offshore pipeline floatation during storms in liquefied soils. *Proc. of the 3rd International Offshore and Polar Engineering Conference (ISOPE), Singapore, 6-11 June 1993, Vol. II, pp. 106-113.*

Vesic, A.S. (1971). Breakout resistance of objects embedded in ocean bottom. Journal of Soil Mechanics and Foundation Division, ASCE, Vol. 97, No. SM9, pp. 1183-1205.